Preprints of the 21st IFAC World Congress (Virtual)
Berlin, Germany, July 12-17, 2020

# Implementation of LPV $\mathcal{H}_\infty$ Loop-Shaping Control for a Variable Stiffness Actuator ⋆

**Lukas Bergmann** * **Lin Liu** * **Nam Pham** * **Berno Misgeld** *
**Steffen Leonhardt** * **Chuong Ngo** *

* *RWTH Aachen University, Medical Information Technology, 52074 Aachen, Germany (e-mail: liu@hia.rwth-aachen.de).*

**Abstract:** Compliant actuators have been increasingly used for active joints in lower-limb exoskeletons or orthoses because they help to guarantee a safe human interaction. One example of such compliant motors is the variable stiffness actuator (VSA). The design of a torque controller for such an actuator is a crucial task in order to provide patients with physical gait assistance and overcome the mechanical limitations of the VSA. Our goal is to implement a torque controller for our mechanical-rotary variable impedance actuator (MeRIA) used in future lower-limb exoskeletons. In the torque control design, we derive a gain-scheduled controller for the polytopic linear parameter-varying (LPV) model of the actuator. This controller is based on the classical $\mathcal{H}_\infty$ loop-shaping approach. Measurements on the hardware-in-the-loop system in time and frequency domain show that the designed controller provides adequate performance over the whole varying stiffness range. Additionally, the controller provides $\mathcal{H}_\infty$ robustness with respect to coprime factor uncertainty for the polytopic system. Thus, the torque controller fulfills major safety requirements, and can further be used for human-in-the-loop tests and applications with a lower-limb exoskeleton.

*Keywords:* H-infinity Loop Shaping, Gain-Scheduling, Polytopic LPV Systems, VSA, Physical Human-Robot Interactions

## 1. INTRODUCTION

Robotic devices, such as lower-limb exoskeletons and active orthoses, are increasingly used for gait training and rehabilitation (Esquenazi and Packel, 2012). Lower-limb exoskeletons are wearable, mechanical structures designed to assist the human gait by providing an additional torque at the subject's joints using electrical or other actuators. These types of exoskeletons are a promising approach for addressing age-related diseases and the rehabilitation for partial gait disorders, e.g., post-stroke hemiplegic patients. However, one challenge for the application of lower-limb exoskeletons is to achieve a safe interaction between human and machine. For this, Vanderborght et al. (2013) suggested the use of Variable Stiffness Actuators (VSA) for applications that require a robot physically interacting with a human subject. A mechanical-rotary variable impedance actuator (MeRIA), developed in our group (Liu et al., 2016), belongs to the category of the VSA. The MeRIA, consists of an adaptable elasticity between the joint motor and the output shaft. One important characteristic of this actuator is the almost decoupled system in terms of torque generation and stiffness variation. Considering the measurable stiffness as an exogenous signal, it is then possible to formulate a linear parameter-varying (LPV) model for the joint actuator.

In VSA control, one challenge is to design a controller that guarantees stability and performance for the whole stiffness range. To avoid this problem, several VSA studies proposed using the interpolating gain-scheduling control, such as Sardellitti et al. (2013), Liu et al. (2018) and Misgeld et al. (2017). In these studies, the gain-scheduling controller was implemented by interpolating a set of linear controllers and then using the measurement of the actuator stiffness to update the controller gains. However, the approach mentioned above cannot ensure stability for the entire domain of the operating point during controller design. Therefore, a post-analysis of stability and performance is required before application.

Unlike these previous approaches, this paper presents the implementation of an LPV controller since the derived VSA model can be represented as a polytopic system. For controlling such systems, Apkarian et al. (1994) and Prempain (2006) proposed an extension to the common $\mathcal{H}_\infty$ loop-shaping control, introduced by Glover and McFarlane (1989), based on polytopic left coprime factorization that guarantees $\mathcal{H}_\infty$ robustness for LPV models. This extension is used to design an LPV $\mathcal{H}_\infty$ loop-shaping torque controller for the MeRIA. The goal is to ensure LPV stability while maintaining a bandwidth larger than the cut-off frequencies of the human knee and hip, which is around 5 Hz and 4 Hz, respectively (Smith, 2007). The effectiveness of the controller was experimentally verified on a test bench. Our results show the advantage of the gain-scheduled LPV controller over classical linear time-invariant controller approaches, that is, the performance preservation over the whole parameter varying range.

⋆ This work was supported in part by the German research foundation under grant LE817/30-1.

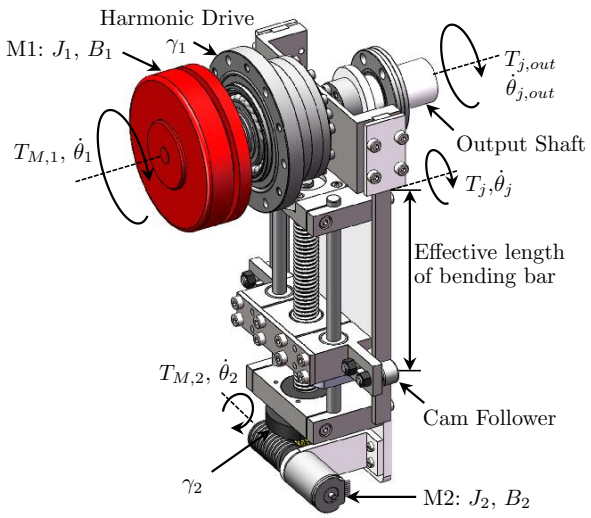


Fig. 1. Drawing of the actuator (MeRIA).

## 2. MODELING OF THE VARIABLE STIFFNESS ACTUATOR

As shown in Figure 1, the MeRIA prototype consists of two motors. The first motor (M1) generates the elastic torque, which is transferred via a Harmonic Drive and two bending bars. The stiffness variation is achieved by adjusting the effective length of the two bending bars. This task is accomplished by the second motor (M2). In Figure 1, $\theta_{j,out}$ describes the rotation position of the joint on the load side. For $i = 1, 2$, $T_{M,i}$ and $\theta_i$ depict the output torque and rotational position of each motor. The torque transferred over the spring is described by $T_j$, while $T_{j,out}$ is the interaction torque between the load and the actuator. For the controller design, the load is assumed to be fixed; thus, holding the condition $\theta_{j,out} = 0$, and assuming $T_{j,out} = T_j$.

Following the system description in Liu et al. (2016), the dynamical equation for M1 of the actuator is given as

$$\frac{d\dot{\theta}_1}{dt} = \frac{K_{emf,1} \cdot I_1}{J_1} - \frac{B_1 \cdot \dot{\theta}_1}{J_1} - \frac{\sigma(\theta_2) \cdot \theta_1}{J_1 \cdot \gamma_1^2}, \tag{1}$$

where $K_{emf,1}$ is the back electromotive force constant of M1, $B_1$ is the bearing resistance coefficient of M1, $J_1$ is the total inertia of M1, and $\gamma_1$ is the transmission coefficient of the Harmonic Drive. The stiffness of the actuator $\sigma(\theta_2)$ is mainly dependent on the position of the cam followers and thus directly dependent on the rotational angle of M2. Based on Hooke's law, the torque $T_{j,out}$ can be calculated as

$$T_{j,out} = \sigma(\theta_2) \cdot \frac{\theta_1}{\gamma_1}. \tag{2}$$

Within the torque loop, a speed controller $K_{PI}(s)$ with proportional and integral action is introduced. The controller law is given as

$$I_1 = (\dot{\theta}_{1,ref} - \dot{\theta}_1) K_{PI}(s), \tag{3}$$

where

$$K_{PI}(s) = K_P + \frac{K_I}{s}. \tag{4}$$

Note that $K_P$ and $K_I$ are chosen such that the inner loop of speed control is faster than the outer torque control loop. By substituting (4) into (3), the input current $I_1$ is reformulated as:

$$I_1 = K_P \cdot \dot{\theta}_{1,ref} + K_I \cdot \theta_{1,ref} - K_P \cdot \dot{\theta}_1 - K_I \cdot \theta_1 \tag{5}$$

By substituting (5) into (1), the dynamics of $\dot{\theta}_1$ (including the PI controller) are obtained:

$$\frac{d\dot{\theta}_1}{dt} = t_1 \cdot \dot{\theta}_{1,ref} + t_2 \cdot \theta_{1,ref} + t_3 \cdot \dot{\theta}_1 + t_4 \cdot \theta_1, \tag{6}$$

where

$$\begin{aligned} t_1 &= \tfrac{K_P \cdot K_{emf,1}}{J_1}, & t_2 &= \tfrac{K_I \cdot K_{emf,1}}{J_1} \\ t_3 &= -\tfrac{K_P \cdot K_{emf,1} + B_1}{J_1}, & t_4 &= -\tfrac{K_I \cdot K_{emf,1} \cdot \gamma^2 + \sigma}{J_1 \cdot \gamma_1^2}. \end{aligned} \tag{7}$$

Between the motor M1 and M2, the coupled torque caused by the change of deflection angle when adjusting the effective length can be neglected, see e.g. Jafari (2014). Thus, a fully decoupled model between joint torque assistance and stiffness variation is obtained.
To control the output torque of the actuator, the dynamic model of M2 is not considered in this context, and the online changeable and measurable stiffness $\sigma(t)$ is treated as an exogenous input. Consequently, the differential equations in (6) can be rewritten as an LPV model in state-space form:

$$\begin{aligned} \dot{\boldsymbol{x}} &= \boldsymbol{A}(\boldsymbol{\sigma}(t))\boldsymbol{x} + \boldsymbol{B}(\boldsymbol{\sigma}(t))u, \\ y &= \boldsymbol{C}(\boldsymbol{\sigma}(t))\boldsymbol{x} + D(\boldsymbol{\sigma}(t))u. \end{aligned} \tag{8}$$

Defining the output $y = T_{j,out}$ and the input $u = \dot{\theta}_{1,ref}$, the state-space matrices of (8) in observable canonical form are given by

$$\begin{aligned} \boldsymbol{x} &= \begin{bmatrix} t_2 \frac{\sigma}{\gamma_1} \theta_{1,ref} \\ \dot{T}_{j,out} - t_3 T_{j,out} \\ T_{j,out} \end{bmatrix}, \ \boldsymbol{A} = \begin{bmatrix} 0 & 0 & 0 \\ 1 & 0 & t_4(\sigma) \\ 0 & 1 & t_3 \end{bmatrix}, \\ \boldsymbol{B} &= \begin{bmatrix} t_2 \cdot \frac{\sigma}{\gamma_1} \\ t_1 \cdot \frac{\sigma}{\gamma_1} \\ 0 \end{bmatrix}, \qquad \boldsymbol{C} = [0 \ 0 \ 1], \qquad D = 0. \end{aligned} \tag{9}$$

The numerical values of the parameters of (9) are provided in Appendix A.

## 3. $\mathcal{H}_\infty$ LOOP-SHAPING CONTROL OF AN LPV SYSTEM

As proposed by Apkarian et al. (1994) and Prempain (2006), the well-known $\mathcal{H}_\infty$ loop-shaping design procedure of McFarlane and Glover can be extended to deal with polytopic LPV Systems in terms of the polytopic left coprime factorization of the shaped LPV plant. The first step of this method is to determine the unique left coprime factorization of a polytopic system by solving formulated Linear Matrix Inequality (LMI) conditions. The second step is to verify sufficient LMI conditions for the existence of an LPV $\mathcal{H}_\infty$ loop-shaping controller. Based on these two steps, a gain-scheduled $\mathcal{H}_\infty$ loop-shaping controller for the polytopic system can be reconstructed.

### *3.1 Polytopic LPV System*

Following Apkarian et al. (1995) and Shamma and Cloutier (1992), an LPV system, as introduced in (8), is a polytopic plant where the state-space matrices are the affine functions with respect to the varying parameter vector $\boldsymbol{\sigma}(t)$. The varying parameter vector $\boldsymbol{\sigma}(t)$ is assumed to be measurable online and each element of the vector is assumed to be bounded with

$$\underline{\sigma}_i < \sigma_i < \overline{\sigma}_i, \tag{10}$$

where $\underline{\sigma}_i$ and $\overline{\sigma}_i$ are a lower and upper bound of the varying parameter $\sigma_i$. The parameter vectors $\boldsymbol{\omega}_j$, which are formed by taking any upper and lower bounds of the vector elements in $\boldsymbol{\sigma}$, are called vertices. There are $m = 2^n$ vertices of the parameter vector $\boldsymbol{\omega}_j$ which span a convex hull (Co), providing an outer boundary for the parameter vector $\boldsymbol{\sigma}$.

$$\boldsymbol{\sigma} \in \mathrm{Co}\left\{\boldsymbol{\omega}_1, \cdots, \boldsymbol{\omega}_m\right\} \tag{11}$$

The transformation of these vertices through an affine parameter-dependent matrix also results in a convex hull, given by the *matrix polytope* (Apkarian et al., 1995). The affine matrices $\boldsymbol{A}(\boldsymbol{\sigma})$, $\boldsymbol{B}(\boldsymbol{\sigma})$, $\boldsymbol{C}(\boldsymbol{\sigma})$, $\boldsymbol{D}(\boldsymbol{\sigma})$ of the LPV system lie within the convex hull that is spanned by matrices $\boldsymbol{A}_j$, $\boldsymbol{B}_j$, $\boldsymbol{C}_j$, $\boldsymbol{D}_j$, where $j$ indicates the index of state-space matrices at vertex $\boldsymbol{\omega}_j$. The state-space matrices of the LPV system (8) are then written as

$$\begin{pmatrix} \boldsymbol{A}(\boldsymbol{\sigma}) & \boldsymbol{B}(\boldsymbol{\sigma}) \\ \boldsymbol{C}(\boldsymbol{\sigma}) & \boldsymbol{D}(\boldsymbol{\sigma}) \end{pmatrix} = \sum_{j=1}^{m} \alpha_j(\boldsymbol{\sigma}) \begin{pmatrix} \boldsymbol{A}_j & \boldsymbol{B}_j \\ \boldsymbol{C}_j & \boldsymbol{D}_j \end{pmatrix}, \tag{12}$$

where for the polytope coordinates the following properties hold: $\alpha_j \geqslant 0$ and $\sum_{j=1}^{m} \alpha_j(\boldsymbol{\sigma}) = 1$.
For the LPV model of the VSA, the parameter vector $\boldsymbol{\sigma}$ simplifies to a scalar describing the variable stiffness. Thus, the polytopic form of the stiffness results in a line segment, which is bounded by two vertices $\omega_1 = \underline{\sigma}$ and $\omega_2 = \overline{\sigma}$. The polytope coordinates are given by:

$$\alpha_1(\sigma) = \frac{\overline{\sigma} - \sigma(t)}{\overline{\sigma} - \underline{\sigma}}, \qquad \alpha_2(\sigma) = \frac{\sigma(t) - \underline{\sigma}}{\overline{\sigma} - \underline{\sigma}}, \tag{13}$$

where $\sigma(t)$ denotes the time-varying stiffness. With the given polytope coordinates $\alpha_1$ and $\alpha_2$, the state-space representation in (9) can be transformed to the polytopic form in (12), where the system matrix $\boldsymbol{A}(\sigma(t))$ and input matrix $\boldsymbol{B}(\sigma(t))$ are parameter-dependent.

### *3.2 Loop-Shaping of the augmented Plant*

The idea of the classical $\mathcal{H}_\infty$ robustly stabilizing controller approach combined with classical loop-shaping described by Glover and McFarlane (1989) is to augment the open-loop plant by a pre- and post-compensator ($W_1$ and $W_2$), and afterward to robustly stabilize the shaped plant $\boldsymbol{G}_s(s)$ using $\mathcal{H}_\infty$ optimization with respect to coprime factor uncertainty (Skogestad and Postlethwaite, 2007). This controller design approach has been extended by Prempain (2006) in order to apply it for the LPV VSA model.
Therefore, consider the shaped plant $\boldsymbol{G}_s(\sigma)$ of the LPV system given by:

$$\boldsymbol{G}_s(\sigma) = W_1 \boldsymbol{G}(\sigma) W_2, \tag{14}$$

where $W_1$ and $W_2$ are a pre- and post-compensator to get the desired shape of the open-loop plant. To derive a stabilizing feedback controller $\boldsymbol{K}_\infty$ of the LPV system, first, a left coprime factorization of the plant is required.

### *3.3 Left Coprime Factors for Polytopic Systems*

For the left coprime factorization of a parameter-dependent system, the state-space representation of the shaped plant $\boldsymbol{G}_s(\sigma)$ must be in the following form, as explained by Prempain (2006):

$$\boldsymbol{G}_s(\sigma) = \left[\begin{array}{c|c} \boldsymbol{A}_s(\sigma) & \boldsymbol{B}_s \\ \hline \boldsymbol{C}_s & \boldsymbol{D}_s \end{array}\right], \tag{15}$$

where

$$\boldsymbol{A}_s(\sigma) = \sum_{i=1}^{m} \alpha_i(\sigma) \boldsymbol{A}_s(\sigma_i), \qquad \alpha_i \geqslant 0, \qquad \sum_{i=1}^{m} \alpha_i = 1. \tag{16}$$

Furthermore, the pairs $(\boldsymbol{A}_s(\sigma), \boldsymbol{B}_s)$ and $(\boldsymbol{C}, \boldsymbol{A}_s(\sigma))$ must be quadratically stabilizable and detectable. Quadratic stabilizability is equivalent to the existence of a state feedback matrix $\boldsymbol{F}$ and a positive definite matrix (denoted by $\succ$) $\boldsymbol{J}_F$ such that:

$$(\boldsymbol{A}_s(\sigma) + \boldsymbol{B}_s\boldsymbol{F})\boldsymbol{J}_F + \boldsymbol{J}_F(\boldsymbol{A}_s(\sigma) + \boldsymbol{B}_s\boldsymbol{F})^T \prec 0, \tag{17}$$

see (Turner and Bates, 2007). Quadratic detectability is equivalent to the existence of an observer matrix $\boldsymbol{L}$ and a positive definite matrix $\boldsymbol{J}_L$ such that

$$\boldsymbol{J}_L(\boldsymbol{A}_s(\sigma) + \boldsymbol{L}\boldsymbol{C}_s) + (\boldsymbol{A}_s(\sigma) + \boldsymbol{L}\boldsymbol{C}_s)^T\boldsymbol{J}_L \prec 0, \tag{18}$$

see (Turner and Bates, 2007).
As shown in Prempain (2006), the normalized left coprime factorization of the shaped plant $\boldsymbol{G}_s(\sigma) = \tilde{\boldsymbol{M}}(\sigma)^{-1}\tilde{\boldsymbol{N}}(\sigma)$ is provided by

$$\left[\tilde{\boldsymbol{M}}(\sigma)\tilde{\boldsymbol{N}}(\sigma)\right] = \left[\begin{array}{c|cc} \boldsymbol{A}_s(\sigma) + \boldsymbol{L}\boldsymbol{C}_s & \boldsymbol{L} & \boldsymbol{B}_s + \boldsymbol{L}\boldsymbol{D}_s \\ \hline \tilde{\boldsymbol{R}}^{-\frac{1}{2}}\boldsymbol{C}_s & \tilde{\boldsymbol{R}}^{-\frac{1}{2}} & \tilde{\boldsymbol{R}}^{-\frac{1}{2}}\boldsymbol{D}_s \end{array}\right], \tag{19}$$

if there exist positive definite, symmetric matrices $\boldsymbol{P}$ and $\boldsymbol{Z}$ solving the optimization problem

$$\begin{gathered} \min trace(\boldsymbol{Z}) \\ \begin{bmatrix} \boldsymbol{P}\boldsymbol{A}_s(\sigma_i) + (\boldsymbol{A}_s(\sigma_i))^T\boldsymbol{P} - \boldsymbol{C}_s^T\boldsymbol{C}_s & \boldsymbol{P}\boldsymbol{B}_s - \boldsymbol{C}_s^T\boldsymbol{D}_s \\ \boldsymbol{B}_s^T\boldsymbol{P} - \boldsymbol{D}_s^T\boldsymbol{C} & -\boldsymbol{R} \end{bmatrix} \prec 0, \\ \text{for } i = 1, \ldots, m \\ \begin{bmatrix} \boldsymbol{Z} & \boldsymbol{I} \\ \boldsymbol{I} & \boldsymbol{P} \end{bmatrix} \succ 0, \end{gathered} \tag{20}$$

with the definition

$$\tilde{\boldsymbol{R}} = \boldsymbol{I} + \boldsymbol{D}_s\boldsymbol{D}_s^T, \qquad \boldsymbol{R} = \boldsymbol{I} + \boldsymbol{D}_s^T\boldsymbol{D}_s$$

and the observer gain

$$\boldsymbol{L} = -(\boldsymbol{B}_s\boldsymbol{D}_s^T + \boldsymbol{P}^{-1}\boldsymbol{C}_s^T)\tilde{\boldsymbol{R}}^{-1}. \tag{21}$$

As stated before, only the matrix $\boldsymbol{A}(\sigma(t))$ is allowed to be parameter-dependent to avoid an infinite number of LMI constraints. However, when observing the LPV model of the VSA, it can be seen that the input matrix $\boldsymbol{B}(\sigma(t))$ is depending on the stiffness parameter. To overcome this fact, the reciprocal value of the online measurable stiffness $\sigma(t)$ is incorporated into the output of the controller (Apkarian et al., 1994; Bolea et al., 2014). The new input matrix can be now given as:

$$B_{nom} = \frac{1}{\sigma(t)} B(\sigma(t)) = \begin{bmatrix} \frac{K_i \cdot K_{emf_1}}{J_1 \cdot \gamma_1} \\ \frac{K_p \cdot K_{emf_1}}{J_1 \cdot \gamma_1} \\ 0 \end{bmatrix}. \tag{22}$$

For shaping the open-loop, the post-compensator $W_2$ is chosen to be 1, and the pre-compensator is selected as a PI structure to shape the desired plant:

$$W_1(s) = W_{1,P} + \frac{W_{1,I}}{s}. \tag{23}$$

The values $W_{1,P} = 70000$ and $W_{1,I} = 7000$ were chosen to ensure a sufficient speed of the control response. Both gains of $W_1$ are remarkably high because the input of (9) is always multiplied by the factor $1/\sigma(t)$. Given the shaped plant with these pre- and post-compensator, the optimization problem given in (20) were solved using the LMI Toolbox in Matlab (Gahinet et al., 1995).

### *3.4 LMI Conditions for Existence of Polytopic LPV $\mathcal{H}_\infty$ Loop-Shaping Controller*

Given the left coprime factorization $(\tilde{\boldsymbol{M}}^{-1}, \tilde{\boldsymbol{N}})$ and the observer gain $\boldsymbol{L}$ of the LPV system with $\boldsymbol{P} \succ 0$, the existence of a dynamic feedback output controller $\boldsymbol{K}(\sigma)$ can be verified using the theorem introduced in Prempain (2006): If there exists a $\gamma > 1$ and positive definite and symmetric matrices $\boldsymbol{Q}$ and $\boldsymbol{S}$ solving the LMIs

$$\boldsymbol{S}(\boldsymbol{A}_s(\sigma_i) + \boldsymbol{L}\boldsymbol{C}_s) + (\boldsymbol{A}_s(\sigma_i) + \boldsymbol{L}\boldsymbol{C}_s)^T\boldsymbol{S} - \gamma \boldsymbol{C}_s^T \tilde{\boldsymbol{R}}^{-1}\boldsymbol{C}_s \prec 0, \quad \text{for } i = 1, \dots, m \tag{24}$$

$$\begin{bmatrix} \boldsymbol{A}_s(\sigma_i)\boldsymbol{Q} + \boldsymbol{Q}(\boldsymbol{A}_s(\sigma_i))^T - \gamma \boldsymbol{B}_s\boldsymbol{B}_s^T & \boldsymbol{Q}\boldsymbol{C}_s^T - \gamma \boldsymbol{B}_s\boldsymbol{D}_s^T & -\boldsymbol{L}\tilde{\boldsymbol{R}}^{\frac{1}{2}} \\ \boldsymbol{C}_s\boldsymbol{Q} - \gamma \boldsymbol{D}_s\boldsymbol{B}_s^T & -\gamma \tilde{\boldsymbol{R}} & \tilde{\boldsymbol{R}}^{\frac{1}{2}} \\ -\tilde{\boldsymbol{R}}^{\frac{1}{2}}\boldsymbol{L}^T & \tilde{\boldsymbol{R}}^{\frac{1}{2}} & -\gamma \boldsymbol{I}_{n_y} \end{bmatrix} \prec 0, \quad \text{for } i = 1, \dots, m \tag{25}$$

$$\begin{bmatrix} \boldsymbol{Q} & \boldsymbol{I} \\ \boldsymbol{I} & \boldsymbol{S} \end{bmatrix} \succ 0 \tag{26}$$

for all vertices of the LPV plant, then there exists a dynamic output feedback LPV controller $\boldsymbol{K}(\sigma)$ fulfilling

$$\left\| \begin{bmatrix} \boldsymbol{K}(\sigma) \\ \boldsymbol{I} \end{bmatrix} (\boldsymbol{I} - \boldsymbol{G}_s(\sigma)\boldsymbol{K}(\sigma))^{-1} \tilde{\boldsymbol{M}}^{-1}(\sigma) \right\|_\infty \leqslant \gamma \tag{27}$$

for all parameter trajectories in the convex polytope of the LPV system. In (27), $\gamma$ is the optimal solution of the $\mathcal{H}_\infty$ norm. The lowest achievable $\gamma$ corresponds to the highest stability margin $\epsilon = 1/\gamma > 0$. This theorem - introduced in Prempain (2006); Prempain and Postlethwaite (2005) - makes use of the bounded real lemma and the classical $\mathcal{H}_\infty$ loop-shaping theory (Skogestad and Postlethwaite, 2007) to prove the existence of an $\mathcal{H}_\infty$ stabilizing controller over the complete range of all varying parameters.
In the case of the VSA, the LMIs in (24)-(26) can be solved using the Matlab LMI toolbox (Gahinet et al., 1995).

### *3.5 Controller Design*

After proving the existence of a dynamic feedback output controller stabilizing the LPV system in the sense of $\mathcal{H}_\infty$ stability, the final step is to design this controller. Therefore, the generalized plant configuration $\boldsymbol{P}_s$ of the LPV system is considered, which is given at a certain vertex $\sigma_i$ by:

$$\boldsymbol{P}_s(\sigma_i) := \left[\begin{array}{c|c|c} \boldsymbol{A}_s(\sigma_i) & -\boldsymbol{L}\tilde{\boldsymbol{R}}^{\frac{1}{2}} & \boldsymbol{B}_s \\ \hline 0 & 0 & \boldsymbol{I}_{n_u} \\ \boldsymbol{C}_s & \tilde{\boldsymbol{R}}^{\frac{1}{2}} & \boldsymbol{D}_s \\ \hline \boldsymbol{C}_s & \tilde{\boldsymbol{R}}^{\frac{1}{2}} & \boldsymbol{D}_s \end{array}\right], \tag{28}$$

where $\boldsymbol{I}_{n_u}$ denotes the unit matrix with the size of the number of inputs. Given the generalized plant $\boldsymbol{P}_s(\sigma_i)$ and $\gamma > 1$, $\boldsymbol{Q} \succ 1$ and $\boldsymbol{S} \succ 1$ from the previous section, one linear, dynamic controller $\boldsymbol{K}_i$ for each vertex of the LPV system can be synthesized by solving an LMI optimization problem based on the bounded real lemma as proposed in Scherer et al. (1997). For the sake of clarity, this algorithm is not discussed in detail. However, the *klmi* function of the LMI toolbox is used to compute a central $\mathcal{H}_\infty$ controller

$$\boldsymbol{K}_i(s) = \boldsymbol{D}_{K_i} + \boldsymbol{C}_{K_i}(s\boldsymbol{I} - \boldsymbol{A}_{K_i})\boldsymbol{B}_{K_i} \hat{=} \left[\begin{array}{c|c} \boldsymbol{A}_{K_i} & \boldsymbol{B}_{K_i} \\ \hline \boldsymbol{C}_{K_i} & \boldsymbol{D}_{K_i} \end{array}\right] \tag{29}$$

Table 1. Characteristics of the closed-loop system with the polytopic LPV $\mathcal{H}_\infty$ controllers

| $\sigma_i$ | 233.5 N m rad$^{-1}$ | 480.9 N m rad$^{-1}$ |
|---|---|---|
| Bandwidth | 11.72 Hz | 11.70 Hz |
| Rise time | 0.03 s | 0.03 s |
| Settling time | 0.06 s | 0.06 s |
| $\gamma$ | 1.54 | 1.54 |

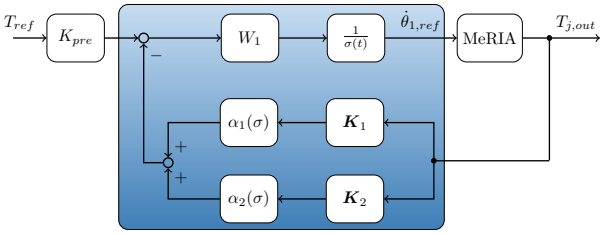


Fig. 2. LPV $\mathcal{H}_\infty$ gain-scheduled torque controller (in blue) for the MeRIA.

at each vertex $i$ that yields a closed-loop gain no larger than the $\gamma$ given in Table 1. The synthesized dynamic $\mathcal{H}_\infty$ controller $K_1$ and $K_2$ for each vertex are given in Appendix B.
The final gain-scheduled output feedback LPV polytopic controller can be provided by:

$$\boldsymbol{K}_\infty(\sigma) = W_2 \left( \sum_{i=1}^{m} \alpha_i \boldsymbol{K}_i \right) W_1, \tag{30}$$

where $W_1$ and $W_2$ denote the pre- and post-compensator in the loop-shaping procedure.
In the case of the VSA, additionally, the pre-factor $1/\sigma(t)$ needs to be considered, which was introduced to make the input matrix of the nominal plant independent of the variable parameter. Thus, the final output feedback controller is given by

$$\begin{aligned} \boldsymbol{K}_\infty(\sigma) &= W_2 \left(\textstyle\sum_{i=1}^{m} \alpha_i \boldsymbol{K}_i\right) \frac{W_1}{\sigma} \\ &= (\alpha_1(\sigma)\boldsymbol{K}_1 + \alpha_2(\sigma)\boldsymbol{K}_2)\frac{W_1}{\sigma}. \end{aligned} \tag{31}$$

The characteristics of the closed-loop system with the two synthesized polytopic $\mathcal{H}_\infty$ controllers at both vertices are given in the Table 1.
The closed-loop system with the designed controller achieves very identical performances at both vertices. Note that, with $\gamma = 1.54$, the polytopic LPV controllers can assure robust stability with the maximal coprime uncertainty of 65% for any arbitrary trajectory of $\sigma(t)$. The control diagram of the final implemented system is depicted in Figure 2, where $K_{pre}$ is a constant pre-gain to ensure a steady-state gain of 1 for reference tracking, according to Skogestad and Postlethwaite (2007).

## 4. CONTROLLER VALIDATION AND DISCUSSION

To evaluate the performance of the $\mathcal{H}_\infty$ gain-scheduled torque controller, real-time control tests were carried out to a test bench introduced by Liu et al. (2016). The experiments presented in the following sections were performed in the case of fixed output, and the output torque signal was measured by a torque sensor (DR-2477, Lorenz GmbH, Alfdorf, GER). The rapid control prototyping process was implemented on a real-time controller board (DS1003, dSPACE GmbH, Paderborn, GER), whereby the sampling frequency was set to 1 kHz.

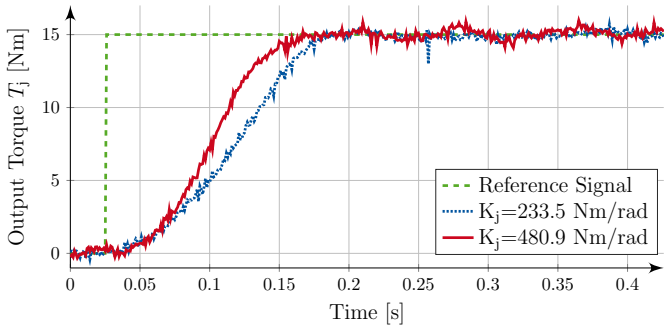


Fig. 3. Experimental result of step response with the gain-scheduled $\mathcal{H}_\infty$ loop-shaping controller at the lowest (blue) and highest (red) possible stiffness.

### *4.1 Step response*

As a reasonable gait assistance torque in lower limb exoskeletons, a step response from 0 N m to 15 N m for the lowest possible stiffness (233.5 N m rad$^{-1}$) and the highest stiffness (480.9 N m rad$^{-1}$) was selected, which is shown in Figure 3. At the highest stiffness, a rising time of 0.13 s for this step was achieved. The step response at the lowest possible stiffness was approximately 0.02 s slower.

The two fixed stiffness values chosen in this test correspond to the operating points of the controllers $\boldsymbol{K}_1$ and $\boldsymbol{K}_2$. In Table 1, however, the calculated rise time for a unit step was equal at both operating points. The mismatch of rise time at low and high stiffness depicted in Figure 3 exposes the non-linearity of the system for different gains of the torque input. Nevertheless, the mismatch in rise time with the input torque of 15 Nm is only about 0.02 s. Therefore, the tracking performance is assumed to be sufficient for the whole range of the variable stiffness.

### *4.2 Sine wave tracking*

To evaluate the performance of the gain-scheduled controller under the influence of a changing stiffness and to validate the requirements for a periodical gait assistance task, we chose a sine wave with a frequency of 1 Hz and an amplitude of 10 N m as reference torque trajectory. Additionally, the stiffness is changing from the highest to the lowest possible value within 7 s, as depicted in the first graph of Figure 4. The output torque (second graph, red) and the torque error (third graph, blue) between measured output and reference trajectory for the polytopic gain-scheduled $\mathcal{H}_\infty$ loop-shaping controller is also depicted in Figure 4. Note that to evaluate the effect of the online varying stiffness on the closed-loop bandwidth, the torque error of sine wave tracking in Figure 4 does not include the mismatch caused by the feedback delay of the real-time system, which was approximated to 0.023 s. The maximum error stays within a range of ±1 N m, while the root mean square error is 0.408 N m.

To emphasize the advantage of the polytopic gain-scheduling approach, the output error with a fixed-gain $\mathcal{H}_\infty$ controller that was designed to assure robust stability for the operating point at $\sigma = 357\,\mathrm{N\,m\,rad^{-1}}$ (Liu et al., 2016) is shown by the green curve in the third graph of Figure 4. The maximum torque error at the high stiffness is 1 N m, and it increases to 1.81 N m with decreasing stiffness. The root mean square error of this performance

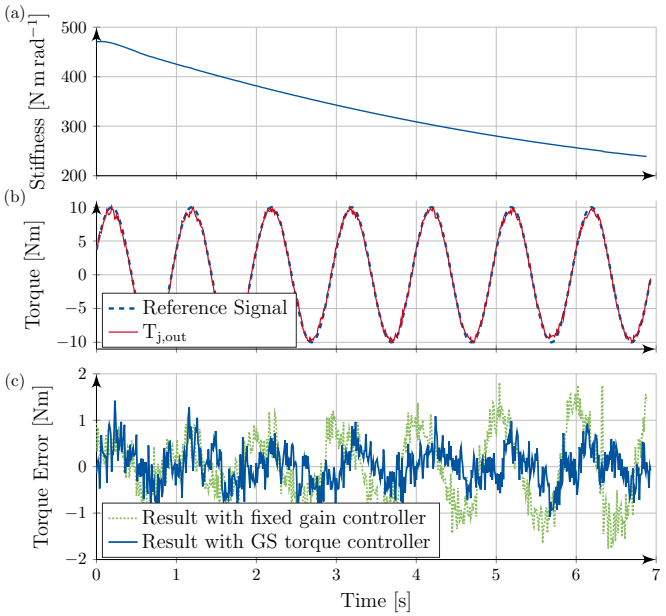


Fig. 4. Experimental result of sine wave tracking with varying stiffness using the gain-scheduled $\mathcal{H}_\infty$ loop-shaping controller. (a) Trajectory of the stiffness variation. (b) Sine wave trajectory and output torque with gain-scheduled controller. (c) Comparison of the output error between the gain-scheduled controller (blue) and the fixed-gain controller (green).

test is 0.731 N m.

The increasing output error for a decreasing stiffness lies in the nature of the fixed-gain controller that controls a system with an increasing time constant. Meaning that the fixed-gain controller loses performance when the bandwidth of the system decreases; and thus, leading to a phase shift and a higher output error. Whereas the gain-scheduling approach assures a certain bandwidth of the closed-loop system when the stiffness decreases. Therefore, the amplitude-attenuation and the phase shift, which would result in larger sine wave tracking errors, are not remarkable in the time domain. It can be concluded that the gain-scheduled controller for the VSA performs well during the sine wave tracking, even with the noisy torque feedback signal and the time-varying stiffness.

### *4.3 Frequency Analysis*

To evaluate the performance of the actuator with the polytopic $\mathcal{H}_\infty$ controller design in the frequency domain, a chirp signal with an input amplitude of 5 N m was exploited as a torque reference. The frequency of chirp signals varied quadratically from 0 Hz to 15 Hz with a sweep time of 40 s. The frequency response is shown in Figure 5.

It can be seen that the bandwidth of the closed-loop system is approximately 7 Hz for the system configuration with the highest stiffness and 5.3 Hz for the lowest stiffness. Furthermore, the highest overshoot with 5 %, in this case, was reached by the system with the lowest stiffness, while the system with the highest stiffness does not have an overshoot.

It must be noticed that the cut-off frequency in this experiment was lower than the one stated in Table 1. This phenomenon is due to the system's non-linearity regarding

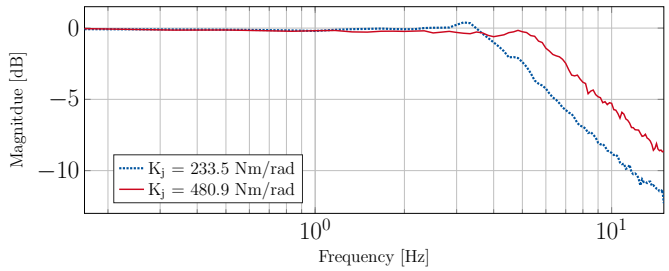


Fig. 5. Frequency response using the $\mathcal{H}_\infty$ loop-shaping controller for a 5 N m chirp signal.

the input gain. Thus, we suggest taking the non-linearity regarding the input amplitude into account at the stage of control design in the future work. Nevertheless, the gain-scheduling controller can provide a bandwidth of the closed-loop system bigger than the cut-off frequency of the human joint over the whole stiffness range.

## 5. CONCLUSION

In this study, we implemented an LPV controller for a VSA based on the classical $\mathcal{H}_\infty$ loop-shaping control. The controller guarantees robust stability with the maximal coprime uncertainty of 65 % while providing a bandwidth equal or larger than the cut-off frequency of a human joint of the lower-limbs. This stability margin holds for the entire stiffness range. The proposed torque control framework can easily be combined with impedance control. The accurate experimental results of torque tracking can also ensure the accuracy of the impedance. These facts enable the use of the MeRIA with the designed controller in gait assistance with lower-limb exoskeletons and in applications like rehabilitation for partial gait disorders and age-related diseases, which is the goal of future research.

## REFERENCES

Apkarian, P., Gahinet, P., and Becker, G. (1995). Self-scheduled $\mathcal{H}_\infty$ Control of Linear Parameter-varying Systems: A Design Example. *Automatica*, 31(9), 1251–1261.

Apkarian, P., Gahinet, P., and Biannic, J.M. (1994). Self-scheduled $\mathcal{H}_\infty$ control of a missile via LMIs. In *Decision and Control, 1994., Proceedings of the 33rd IEEE Conference on*, volume 4, 3312–3317 vol.4.

Bolea, Y., Puig, V., and Blesa, J. (2014). Gain-scheduled Smith predictor PID-based LPV controller for open-flow canal control. *IEEE transactions on control systems technology*, 22(2), 468–477.

Esquenazi, A. and Packel, A. (2012). Robotic-Assisted Gait Training and Restoration. *American Journal of Physical Medicine & Rehabilitation*, 91(11).

Gahinet, P., Nemirovski, A., Laub, A.J., and Chilali, M. (1995). LMI Control Toolbox: For use with MATLAB. *The Math Works*.

Glover, K. and McFarlane, D. (1989). Robust stabilization of normalized coprime factor plant descriptions with $\mathcal{H}_\infty$ bounded uncertainty. *IEEE Transactions on Automatic Control*, 34(8).

Jafari, A. (2014). Coupling between the Output Force and Stiffness in Different Variable Stiffness Actuators. *Actuators*, 3(3), 270.

Liu, L., Leonhardt, S., and Misgeld, B.J.E. (2016). Design and control of a mechanical rotary variable impedance actuator. *Mechatronics*, 39, 226–236.

Liu, L., Leonhardt, S., and Misgeld, B.J. (2018). Experimental validation of a torque-controlled variable stiffness actuator tuned by gain scheduling. *IEEE/ASME Transactions on Mechatronics*, 23(5), 2109–2120.

Misgeld, B.J., Hewing, L., Liu, L., and Leonhardt, S. (2017). Robust gain-scheduled control of variable stiffness actuators. *IFAC-PapersOnLine*, 50(1), 8804–8809.

Prempain, E. (2006). Gain-scheduling $\mathcal{H}_\infty$ loop shaping control of linear parameter-varying systems. *IFAC Proceedings Volumes (IFAC-PapersOnline)*, 5, 215–219.

Prempain, E. and Postlethwaite, I. (2005). Static $\mathcal{H}_\infty$ Loop Shaping Control of a Fly-by-wire Helicopter. *Automatica*, 51, 1517–1528.

Sardellitti, I., Medrano-Cerda, G.A., Tsagarakis, N., Jafari, A., and Caldwell, D.G. (2013). Gain scheduling control for a class of variable stiffness actuators based on lever mechanisms. *IEEE Transactions on Robotics*, 29(3), 791–798.

Scherer, C., Gahinet, P., and Chilali, M. (1997). Multiobjective output-feedback control via LMI optimization. *IEEE Transactions on automatic control*, 42(7), 896–911.

Shamma, J.S. and Cloutier, J.R. (1992). A linear parameter varying approach to gain scheduled missile autopilot design. In *1992 American Control Conference*, 1317–1321. IEEE.

Skogestad, S. and Postlethwaite, I. (2007). *Multivariable feedback control: analysis and design*, volume 2. Wiley New York.

Smith, J.D. (2007). *Effects of prosthesis inertia on the mechanics and energetics of amputee locomotion*. dissertation, Pennsylvania State University.

Turner, M.C. and Bates, D.G. (2007). Mathematical methods for robust and nonlinear control. *Book series on control systems. Springer, Berlin*.

Vanderborght, B. et al. (2013). Variable impedance actuators: A review. *Robotics and Autonomous Systems*, 61(12), 1601–1614.

## Appendix A. PARAMETER OF THE VSA

Table A.1. Nominal values of the dynamic model of the MeRIA

| Parameter | Value | Unit |
|---|---|---|
| $K_{emf_1}$ | 0.0707 | $[\mathrm{V\,s\,rad^{-1}}]$ |
| $J_1$ | $3.435 \cdot 10^{-4}$ | $[\mathrm{kg^2\,m}]$ |
| $B_1$ | 0.01 | $[\mathrm{N\,m\,s\,rad^{-1}}]$ |
| $\gamma_1$ | 100 | [-] |
| $K_P$ | 0.12 | $[\mathrm{A\,rad^{-1}}]$ |
| $K_I$ | 26 | $[\mathrm{A\,rad^{-1}\,s^{-1}}]$ |
| $K_{pre}$ | 0.808 | [-] |

## Appendix B. RECONSTRUCTED $\mathcal{H}_\infty$ CONTROLLER AT EACH VERTEX

$$\boldsymbol{K}_1 = \left[\begin{array}{ccc|c} -0.1139 & -94.94 & -672.4 & -4.456 \\ 4.737 & -8.471 & 141.6 & 0.6534 \\ 33.43 & -257.6 & -406.5 & -4.572 \\ \hline -0.1849 & 6.515 & 38.16 & 1.118 \end{array}\right] \tag{B.1}$$

$$\boldsymbol{K}_2 = \left[\begin{array}{ccc|c} -0.05219 & -94.88 & -673 & -4.455 \\ 4.72 & -8.492 & 141.8 & 0.6529 \\ 33.43 & -257.6 & -406.4 & -4.57 \\ \hline -0.1867 & 6.513 & 38.18 & 1.118 \end{array}\right] \tag{B.2}$$